The 1.9 Å Crystal Structure of Alanine Racemase from *Mycobacterium tuberculosis* Contains a Conserved Entryway into the Active Site[†,‡]

Pierre LeMagueres,[§] Hookang Im,[§] Jerry Ebalunode,[§] Ulrich Strych,[§] Michael J. Benedik,[||] James M. Briggs,[§] Harold Kohn,[⊥] and Kurt L. Krause*[,§,@]

Department of Biology and Biochemistry, University of Houston, Houston, Texas 77204-5001, Department of Biology, Texas A&M University, College Station, Texas 77843-3258, Division of Medicinal Chemistry and Natural Products, School of Pharmacy, University of North Carolina, Chapel Hill, North Carolina 27599-7360, and Section of Infectious Diseases, Department of Medicine, Baylor College of Medicine, Houston, Texas 77030

Received June 27, 2004; Revised Manuscript Received October 22, 2004

ABSTRACT: We report the crystal structure of alanine racemase from *Mycobacterium tuberculosis* (Alr_{Mtb}) at 1.9 Å resolution. In our structure, Alr_{Mtb} is found to be a dimer formed by two crystallographically different monomers, each comprising 384 residues. The domain makeup of each monomer is similar to that of *Bacillus* and *Pseudomonas* alanine racemases and includes both an α/β-barrel at the N-terminus and a C-terminus primarily made of β-strands. The hinge angle between these two domains is unique for Alr_{Mtb}, but the active site geometry is conserved. In Alr_{Mtb}, the PLP cofactor is covalently bound to the protein via an internal aldimine bond with Lys42. No guest substrate is noted in its active site, although some residual electron density is observed in the enzyme's active site pocket. Analysis of the active site pocket, in the context of other known alanine racemases, allows us to propose the inclusion of conserved residues found at the entrance to the binding pocket as additional targets in ongoing structure-aided drug design efforts. Also, as observed in other alanine racemase structures, PLP adopts a conformation that significantly distorts the planarity of the extended conjugated system between the PLP ring and the internal aldimine bond.

With approximately one-third of the world's population infected with the tuberculosis bacillus, tuberculosis (TB)[1] is the deadliest infectious disease for human adults (*1*). Every year, about 8 million people will develop active TB and between 2 and 3 million will succumb to this illness (*2*, *3*). Although tuberculosis disproportionately affects the Third World, it is still a major concern in the United States. In the early 1990s, a resurgence of tuberculosis in the United States took place primarily due to infection involving patients with AIDS, and was reflected in 64 000 excess cases of tuberculosis reported in this country through 1993 (*4*). Estimates of the cost to society of these AIDS-related tuberculosis cases have reached hundreds of millions of dollars (*5*). As a result, advances in the treatment of tuberculosis would have enormous public health benefits.

Coupled with this increase in the incidence of tuberculosis has been a major increase in multidrug resistance. It is estimated that ∼5−10% of tuberculosis cases in the United States are caused by organisms that are resistant to one or more first-line anti-tuberculosis agents (*6*), and up to 15% among AIDS patients (*7*). Treatment of MDR tuberculosis is difficult and so costly that both the Centers for Disease Control and Prevention and the National Institutes of Health have listed this agent as a bioterrorism threat (*8*−*11*). Despite a clear need for new agents, no new drugs specifically marketed to target tuberculosis have been introduced in the United States in more than three decades.

Since the sequencing of the genome of *Mycobacterium tuberculosis* (*12*), great effort has been devoted to the study of promising targets for the development of new antimycobacterial agents (*13*, *14*). One of these proteins, alanine racemase (Alr) (EC 5.1.1.1), is a pyridoxal 5′-phosphate (PLP)-containing enzyme essential for the growth of bacteria. It catalyzes the racemization of L-alanine into D-alanine, a key building block in the biosynthesis of the peptidoglycan layer in bacterial cell walls. Because Alr is essentially absent in eukaryotes but ubiquitous among prokaryotes, it has long been an attractive target for antimicrobial development (*15*, *16*). As a result, a number of alanine racemase inhibitors have been synthesized, and most are structural analogues of D-alanine (*17*). However, these compounds are not specific for Alr, but also act on other PLP-containing enzymes, including those found in humans (*18*, *19*). The antibiotic D-cycloserine is an efficient inhibitor of alanine racemase. It is still marketed as a drug for tuberculosis, but its clinical

[†] This publication was supported, in part, by grants from the National Institutes of Health (AI-46340) the W. M. Keck Foundation, and the Robert A. Welch Foundation.

[‡] The coordinates have been deposited in the Protein Data Bank as entry 1XFC.

* To whom correspondence should be addressed. Telephone: (713) 743-8370. Fax: (713) 743-8373. E-mail: kkrause@uh.edu.

[§] University of Houston.

[||] Texas A&M University.

[⊥] University of North Carolina.

[@] Baylor College of Medicine.

[1] Abbreviations: Alr, alanine racemase; Alr_{Mtb}, alanine racemase from *M. tuberculosis*; Alr_{Bst}, alanine racemase from *G. stearothermophilus*; CCD, charge-coupled device; $DadX_{Pao}$, catabolic alanine racemase from *P. aeruginosa*; DCS, D-cycloserine; MAD, multiwavelength anomalous dispersion; MDR, multidrug resistant; PLP, pyridoxal 5′-phosphate; rms, root-mean-square; TB, tuberculosis.

10.1021/bi0486583 CCC: $30.25
Published on Web 01/08/2005

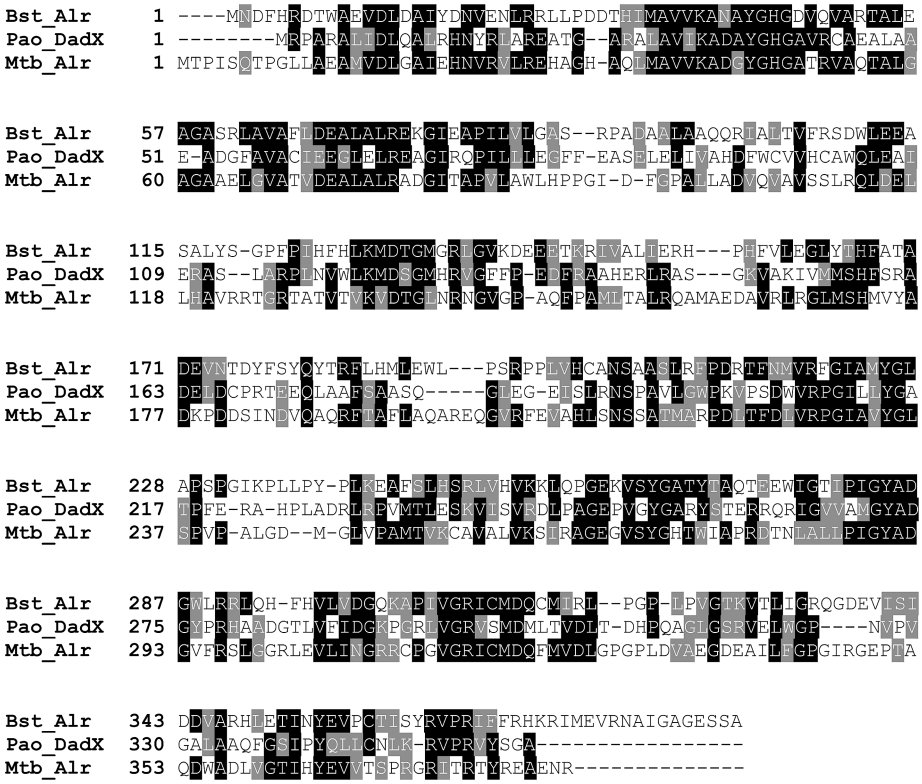

FIGURE 1: Structure-based sequence alignment of alanine racemases from *M. tuberculosis* (Alr_{Mtb}), *P. aeruginosa* ($DadX_{Pao}$), and *G. stearothermophilus* (Alr_{Bst}). The sequences were aligned in QUANTA using a least-squares fit of the C_α atoms and adjusted manually upon examination of the superimposed structures.

use is severely restricted because of serious side effects, such as central nervous system toxicity (*20*−*22*).

Structural studies on alanine racemase from *Geobacillus stearothermophilus* (formerly *Bacillus)* (*23*, *24*) have established that Alr is a homodimeric enzyme, each monomer consisting of two different domains, an α/β-barrel at the N-terminus and a C-terminal domain with a novel architecture composed primarily of β-strands. The core of the α/β-barrel constitutes the active site in which the PLP cofactor forms an internal aldimine linkage with a lysine residue. Two nearby arginine residues and one tyrosine have been found to be involved in hydrogen bonding with both the PLP cofactor and all inhibitors or substrate analogues used in structural studies to date. (*23*−*27*). Further support for these residues having a role in the enzyme's catalytic mechanism has come from structural studies conducted with substrate analogues (*27*). Structures of Alr with the covalent inhibitors alanine phosphonate and D-cycloserine have demonstrated that inhibition of Alr often occurs via the formation of a stable covalent linkage with PLP (*28*, *29*), which is similar to other PLP enzymes (*30*, *31*).

We recently reported the 1.45 Å crystal structure of alanine racemase (DadX) from *Pseudomonas aeruginosa*, an important human pathogen (*26*). While most of the structural characteristics of Alr from *Geobacillus* are conserved in the DadX structure, we reported a serendipitous finding involving PLP. We presented structural evidence of both internal and external aldimine linkages involving PLP in the active site of the DadX crystal structure. This evidence was interpreted to represent a dynamic interchange between an internal aldimine involving lysine and an external aldimine involving an unanticipated guest substrate.

We report here the crystal structure of alanine racemase from *M. tuberculosis* (Alr_{Mtb}) at 1.9 Å resolution. The levels of amino acid sequence identity between Alr_{Mtb} and the two other published alanine racemase structures, DadX from *P. aeruginosa* ($DadX_{Pao}$) (*26*) and Alr from *G. stearothermophilus* (Alr_{Bst}) (*23*), are 32 and 34%, respectively (Figure 1). As expected, the structures of all three enzymes are similar, and a detailed comparison is presented. In addition, we now report that residues found outside of the active site but within the entryway leading to the active site are strongly conserved. We propose that these residues be incorporated into current drug design efforts that could allow for the rational design of larger and potentially more specific inhibitors.

MATERIALS AND METHODS

Purification. Escherichia coli BL21(DE3) containing pMB1909 (alr_{TB}) (*32*) was grown in LB medium with chloramphenicol (30 μg/mL) and kanamycin (50 μg/mL) at 37 °C. At an OD_{600} of 0.6−0.9, 0.5 mM IPTG was added. Cells were grown overnight at 30 °C and harvested by centrifugation. Cell pellets were resuspended in 20 mM Tris (pH 8.0) and 0.5 mM PLP. Cells were lysed using a Spectronic French press at 16 000 psi, and cell debris was removed by centrifugation. Less than 5% of Alr_{Mtb} was found in the soluble fraction. After $(NH_4)_2SO_4$ 25 and 60% cuts, protein pellets were resuspended and dialyzed against 20 mM Tris (pH 8.0), loaded on a Pharmacia Biotech Q-Sepharose high-performance anion exchange column, and eluted with a NaCl gradient. Pooled fractions containing the highest specific activity were loaded on a Pharmacia Hi-Prep Phenyl (low sub) hydrophobic interaction chromatography column

Table 1: Data Collection and Processing Statistics for the MAD and Native Data Sets of Alr_{Mtb}

	MAD 1	MAD 2	MAD 3	MAD 4	native
λ (Å)	0.9788	0.9790	0.9562	0.9809	0.9160
resolution (Å)		2.20			1.80
mosaicity		0.50			0.65
no. of reflections observed $>1\sigma$	432376	446744	431524	336135	779600
no. of unique reflections $>1\sigma$	35817	37506	36020	36242	67592
R_{merge}[a] (%)	6.9	6.4	5.1	3.7	6.0 (67.2)
completeness (%)	91.8	95.8	92.1	92.1	99.3 (95.6)
$\langle I/\sigma \rangle$	30.3	34.3	41.6	50.9	34.5 (2.6)

[a] $R_{merge} = \sum|I_{obs} - I_{avg}|/\sum|I_{avg}|$.

and eluted with a 1 to 0 M $(NH_4)_2SO_4$ gradient. Peak fractions were further purified on a Pharmacia Superdex 200 Prep Grade column. For the selenomethionine-containing protein, *E. coli* B834 (Novagen) was used as the host strain and cells were grown at 37 °C in M9 medium supplemented with kanamycin (50 μg/mL) and selenomethionine.

Crystallization. Native and selenomethionine-containing Alr_{Mtb} (20 mg/mL) were crystallized at 4 °C in sitting drops equilibrated versus 25% PEG400, 0.3 M $CaCl_2$, and 0.1 M sodium carbonate-bicarbonate (pH 9.2). Hexagonal, deeply yellow crystals with dimensions of 0.3 mm × 0.2 mm × 0.2 mm were obtained in space group $P4_12_12$ with the following unit cell parameters: $a = b = 164.78$ Å and $c = 57.88$ Å.

Data Collection and Processing. Multiple anomalous dispersion (MAD) data sets were collected at beamline 14-ID-B of the BioCARS sector of the Advanced Photon Source at Argonne National Laboratory (Argonne, IL). Four different MAD data sets were collected at −180 °C on a single crystal to a resolution of 2.2 Å using a MAR CCD detector. Native data were collected to 1.80 Å resolution on a wild-type crystal at beamline F1 of the Cornell High Energy Synchrotron Source using a Q4 CCD detector. All data were integrated, scaled, reduced, and merged using the HKL package (*33*). Collection and processing statistics for the MAD and native data sets are listed in Table 1.

Structure Determination and Refinement. Assuming two monomers per asymmetric unit, as suggested by a Matthews coefficient of 2.65 with a solvent content of 53%, 19 of the 20 expected selenium atoms were readily located using SOLVE (*34*). The data were initially phased to 2.2 Å resolution with an overall mean figure of merit of 65%. The experimental phases as determined by SOLVE and the entire native data set were input into ARP/wARP in the *warpNtrace* mode for the tracing of the protein (*35*, *36*). A total of 10 iterations, consisting of one cycle of model building and 10 cycles of positional and B_{iso} refinement, yielded 89% of the entire trace of the protein (681 of 768 residues) with a connectivity index of 97% and an *R*-factor of 21.1%. Missing residues (~40 in each monomer) were primarily located in the N- and C-termini, but some of them were also located in the active site. The side chains of those residues that could be built were fitted into the corresponding electron density using the side chains docking script *side_dock.sh* of ARP/wARP and the amino acid sequence (*37*). Next, solvent molecules were removed, and the protein model was submitted to 20 cycles of positional refinement with all *B*-factors fixed at 20 Å^2, followed by 20 cycles of positional and B_{iso} refinement using SHELXL (*38*) with standard restraints using data to 1.95 Å. At this intermediate state, the values of *R* and R_{free} (calculated on 3% of the whole data set) were 29.9 and 35.0%, respectively. Careful examination of the electron density maps obtained with coefficients $2F_{obs} - F_{calc}$ (Sigma-A map) and $F_{obs} - F_{calc}$ (Sigma-D map) (*38*) in O (*39*) revealed additional interpretable density and allowed for the inclusion of 41 more residues, yielding *R* and R_{free} values of 28.2 and 34.2%, respectively. Placement of the PLP cofactors in both monomers further decreased *R* and R_{free} to 27.7 and 33.7%, respectively. By combining ARP/wARP in the *solvent building* mode with SHELXL refinements, we located a total of 350 waters, yielding values for *R* and R_{free} of 22.9 and 28.3%, respectively. Extension of the data to 1.90 Å, followed by refinement of the anisotropic scaling parameter and addition of a solvent mask, all in SHELXL, further decreased the *R* and R_{free} parameters to their final values of 20.4 and 25.4%, respectively, for 55 001 reflections between 30 and 1.90 Å for which $I > 2\sigma_{(I)}$ (Table 2). Further extension of the data to 1.80 Å was attempted but did not improve the density, the *R* factor, or any other statistics. Because the shell of data from 1.90 to 1.80 Å had higher R_{merge} values than other shells, we were not surprised by this result and chose to restrict the data to 1.90 Å.

Table 2: Final Refinement Statistics for Alr_{Mtb} at 1.9 Å Resolution

R factor[a] (%)	20.4
R_{free} (%) (for 1747 reflections)	25.4
average *B* factor (Å^2)[b]	
main chain	25.5
side chain	31.5
PLP	21.9
waters	32.4
rms deviations	
bond lengths (Å)	0.006
bond angles (deg)	1.9
no. of reflections $>2\sigma$	55001
no. of residues	722
no. of protein atoms	5360
no. of PLP atoms	30
no. of water molecules	350

[a] *R*-factor $= \sum|F_{obs} - F_{calc}|/\sum|F_{obs}|$. [b] All isotropic model.

The final Alr_{Mtb} structure contains two crystallographically distinct monomers with a total of 722 residues, 5360 non-hydrogen protein atoms, 350 water molecules, and 30 non-hydrogen PLP atoms. The root-mean-square deviations from ideality for bond lengths and angles are 0.006 Å and 1.9°, respectively. Electron density is missing for residues located at the N- and C-termini of both monomers (residues 1−10 and 382−384) and for residues 174−178 in monomer A and residues 264−278 in monomer B. These residues were not included in the structure. Electron density for the side chain of Arg140 of monomer A was also missing and included as alanine in the final refinement.

RESULTS AND DISCUSSION

Description of the Overall Structure. The structure of Alr from *M. tuberculosis* (Alr_{Mtb}) is a homodimer formed by a head-to-tail association of two monomers (Figure 2). The monomers are crystallographically distinct but very similar in geometry, as evidenced by a low rms difference of 0.56 Å obtained for their C_α atoms after least-squares superposi-

FIGURE 2: Ribbon diagram of the dimer of the alanine racemase from *M. tuberculosis*. The gray spheres represent the side chain of Lys42 and the PLP cofactor.

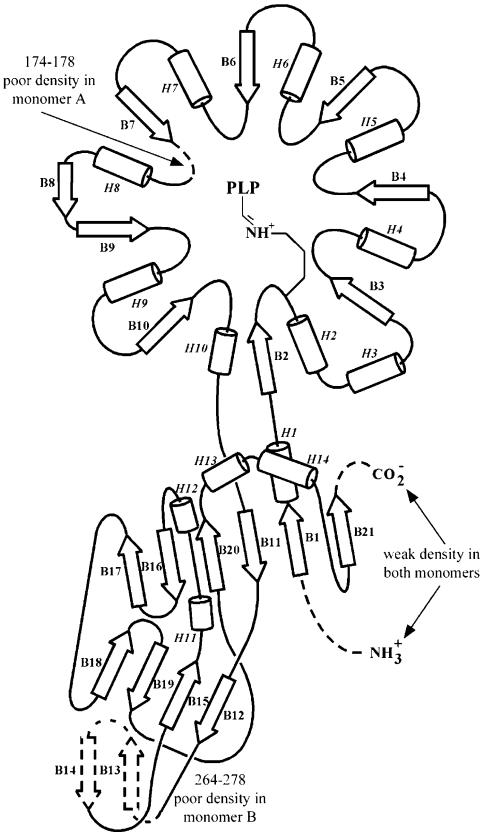

FIGURE 3: Topology diagram representing the secondary structure of Alr_{Mtb} (based on ref *23*).

Table 3: Average rms Differences (Å) among the C_α Atoms of Alr_{Mtb}, $DadX_{Pao}$, and Alr_{Bst}

	whole monomers	N-terminal domains	C-terminal domains	active site
		Alr_{Mtb}		
$DadX_{Pao}$	2.11[a]	1.73[a]	1.59[a]	0.85[b]
Alr_{Bst}	2.06[a]	1.76[a]	1.79[a]	0.72[b]
		$DadX_{Pao}$		
Alr_{Bst}	3.26	1.88	1.63	0.86

[a] Calculated using monomer A. [b] Calculated using the active site composed of the N-terminal domain of monomer B and the C-terminal domain of monomer A. It contains residues 40−46, 64−68, 85−89, 104−108, 129−142, 167−175, 207−214, 225−232, and 361−368 from monomer B and residues 269′−272′ and 316′−321′ from monomer A.

tion. Each Alr_{Mtb} monomer consists of two different domains. The N-terminal domain is an eight-stranded α/β-barrel formed by residues 1−246. The C-terminal domain comprises residues 247−384 and contains predominantly β-structure. When the structure is viewed from the side, there is an angle of approximately 130° between the N- and C-terminal domains. The secondary structure and overall fold of Alr_{Mtb} are very similar to those observed in $DadX_{Pao}$ and Alr_{Bst} (Figure 3), confirming a strong architectural resemblance between prokaryotic alanine racemases. In Table 3, the rms differences between the N- and C-terminal domains of Alr_{Mtb}, $DadX_{Pao}$, and Alr_{Bst}, each superimposed separately, are reported. These rms values all range between 1.6 and 1.9 Å and indicate that notable structural differences between the individual domains exist despite their strong topological similarity.

As shown in Figure 4, the Alr_{Mtb} monomer cannot be superimposed onto that of $DadX_{Pao}$ or Alr_{Bst} as a whole. Superposition of the α/β-barrel of Alr_{Mtb} with those of the two other alanine racemases results in their β-domains being significantly displaced from each other. In Alr_{Mtb}, this shift relative to Alr_{Bst} is due to an 8° rotation around an axis that passes through Glu365. Interestingly, the interdomain angle found in Alr_{Mtb} is approximately one-half of the 15° interdomain angle recently reported for $DadX_{Pao}$ (Figure 4) (*26*). For the $DadX_{Pao}$ and Alr_{Bst} structures, these distinct domain orientations appear to result from hydrogen bonding observed between the N- and C-terminal tails of opposite monomers (*26*). Although this may also be true for Alr_{Mtb}, the density in this region is not very clear. In our analysis, crystal packing does not have any influence on the hinge angle.

N-Terminal Domain (residues 1−246). At the N-terminal domain, structural differences between Alr_{Mtb} and $DadX_{Pao}$ and Alr_{Bst} occur near the N-terminus and in some helices and loops located in the periphery of the α/β-barrel (Figure 5a). However, the core residues that form the active site of all three proteins superimpose very well (Figure 6) with rms differences of 0.85 and 0.72 Å between the C_α atoms of Alr_{Mtb} and those of $DadX_{Pao}$ and Alr_{Bst}, respectively. In the N-terminus, the first Alr_{Mtb} residue observed, Leu11, matches Pro3 of $DadX_{Pao}$ and Asp7 of Alr_{Bst} with rms differences of 3.9 and 1.0 Å, respectively. Val16 of Alr_{Mtb} and Ile8 of

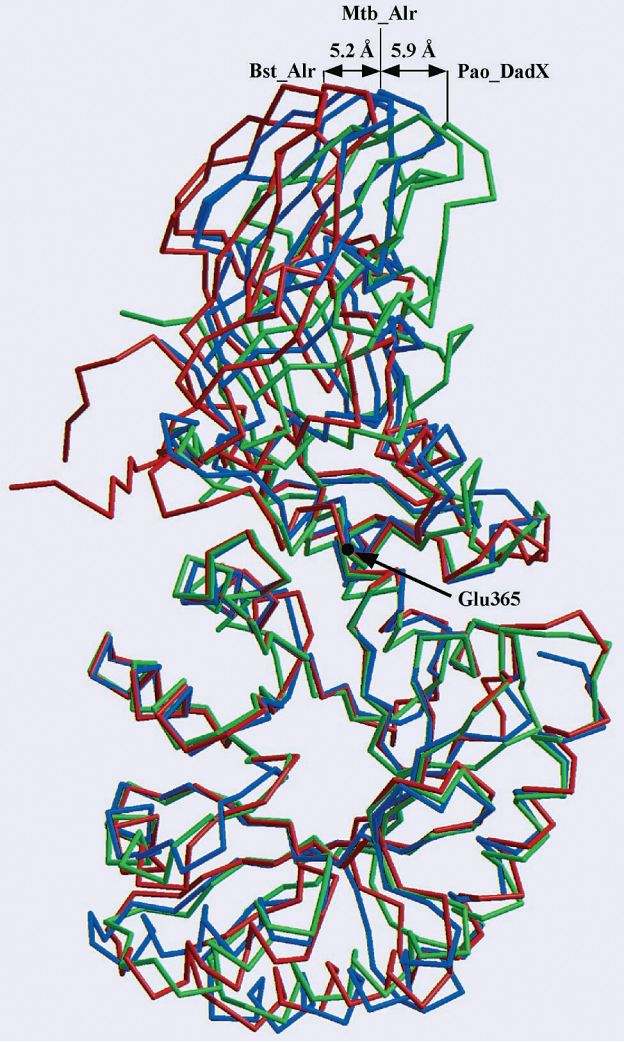

FIGURE 4: Superposition of the monomers of Alr_{Mtb} (blue), $DadX_{Pao}$ (green), and Alr_{Bst} (red) obtained after a least-squares fit of the C_α atoms from the N-terminal domains exclusively. The different interdomain rotation angles for all three proteins are apparent. At the top of the figure, the distance between structurally equivalent residues is reported.

$DadX_{Pao}$ are the first residues with rms differences of less than 1 Å (0.55 Å) for these two enzymes.

Most regions of Alr_{Mtb} that have high rms differences with $DadX_{Pao}$ and Alr_{Bst} are directly related to deletions and insertions (Figure 1). For instance, the loop between H1 and B2 is one residue longer in Alr_{Mtb} than in $DadX_{Pao}$ (His34 inserted) but one residue shorter than in Alr_{Bst} (Asp31 deleted). As a result, the Alr_{Mtb} trace for this loop is distinct from that of $DadX_{Pao}$ and Alr_{Bst}. Similarly, the turns between H3 and B3, and between B4 and H5 contain insertions or deletions that result in locally higher rms differences with $DadX_{Pao}$ and Alr_{Bst}. Interestingly, due to insertions between residues 120 and 130, 160 and 170, and 200 and 210, H6−H8 are all approximately one turn longer in Alr_{Mtb}. On the other hand, since the region of residues 240−249 contains a deletion compared to $DadX_{Pao}$ and Alr_{Bst}, H11 is replaced with a hairpin loop in Alr_{Mtb}.

C-Terminal Domain (residues 247−384). The β-structure of the C-terminal domain reported for $DadX_{Pao}$ (*26*) and Alr_{Bst} (*23*) is conserved in Alr_{Mtb} (Figure 5b). The few structural differences that are observed appear in regions that do not interact with the other monomer upon dimerization. For example, the loops labeled 1 (between B19 and B20 in Alr_{Mtb}) and 2 (immediately before H13 in Alr_{Mtb}) in Figure 5b contain a different number of residues in all three alanine racemases and adopt somewhat different orientations in all three structures.

Another region of significant structural variability is located at the extreme C-terminus. For example, the last residue observed in Alr_{Mtb}, Ala381, has a high rms difference with its equivalent residues, Ala357 of $DadX_{Pao}$ (5.3 Å) and His371 of Alr_{Bst} (3.0 Å). These termini differ in overall length with Alr_{Mtb} containing three more residues (382−384) than $DadX_{Pao}$ but 14 fewer residues than Alr_{Bst}. As a result, the last β-strand (B20) of Alr_{Bst} is absent in both Alr_{Mtb} and $DadX_{Pao}$. These structural differences likely contribute to the variable interdomain angle that has been noted in alanine racemases, because they are involved in hydrogen bonding between the N- and C-termini of opposite monomers.

To illustrate, consider $Asn379_{AlrBst}$, a residue involved in one of the three intermonomer hydrogen bonds that contributes to the interdomain angle in alanine racemase. This residue or its equivalent is lacking in both Alr_{Mtb} and $DadX_{Pao}$. In addition, Phe4 of Alr_{Bst}, another residue involved in intermonomer hydrogen bonding, is missing in $DadX_{Pao}$, but has an equivalent in Alr_{Mtb}, probably Pro8, although density is weak in this region. As a result, it is possible that, of the three intermonomer hydrogen bonds observed in Alr_{Bst}, none are present in $DadX_{Pao}$, but one or two may be present in Alr_{Mtb} based on sequence homology. This bonding pattern would then potentially explain the different interdomain rotations found in all three proteins.

Active Site. The active site of the protein is located in the center of the α/β-barrel and contains a PLP cofactor covalently linked to Lys42. The primary substrate binding cavity in Alr_{Mtb} is ~5.5 Å × 5.0 Å × 2.5 Å and lies adjacent to the PLP cofactor. Acetate, propionate, alanine phosphonate, D-cycloserine, and the putative substrate in DadX are all located in this region in the structures of complexes reported to date (*23*, *24*, *26*, *28*, *29*, *40*). This cavity is delimited on one side by PLP, the side chain of Met319′, and the side chains of Tyr46 and Tyr364. Overall, the geometry of the active site of Alr_{Mtb} closely matches that of $DadX_{Pao}$ and Alr_{Bst} (Figure 6). The rms differences between the C_α atoms of the active site residues in Alr_{Mtb} and their equivalent in $DadX_{Pao}$ and Alr_{Bst} are 0.85 and 0.72 Å, respectively (Table 3). The levels of sequence identity between the active site residues of Alr_{Mtb} and those of $DadX_{Pao}$ and Alr_{Bst} are 44 and 50%, respectively, while it is 47% between $DadX_{Pao}$ and Alr_{Bst}. There is clear contiguous electron density between the protein Lys42 and the C4′ atom of PLP, characteristic of an internal aldimine bond between the protein and the cofactor. Consistent with several previous alanine racemase structural reports, there is some weak density at 3σ in the region where inhibitors and substrates bind, but it is too weak to allow any interpretation.

From this active site cavity, a second cavity on the opposite side of PLP is accessible. This cavity, first reported in $DadX_{Pao}$, has dimensions of 6.0 Å × 4.5 Å × 7.5 Å. In Alr_{Bst}, this cavity contains four water molecules, whereas in $DadX_{Pao}$, it contains three solvent atoms. In Alr_{Mtb}, the presence of Trp88 in this cavity reduces the free space, and only two water molecules are found. One of these two waters

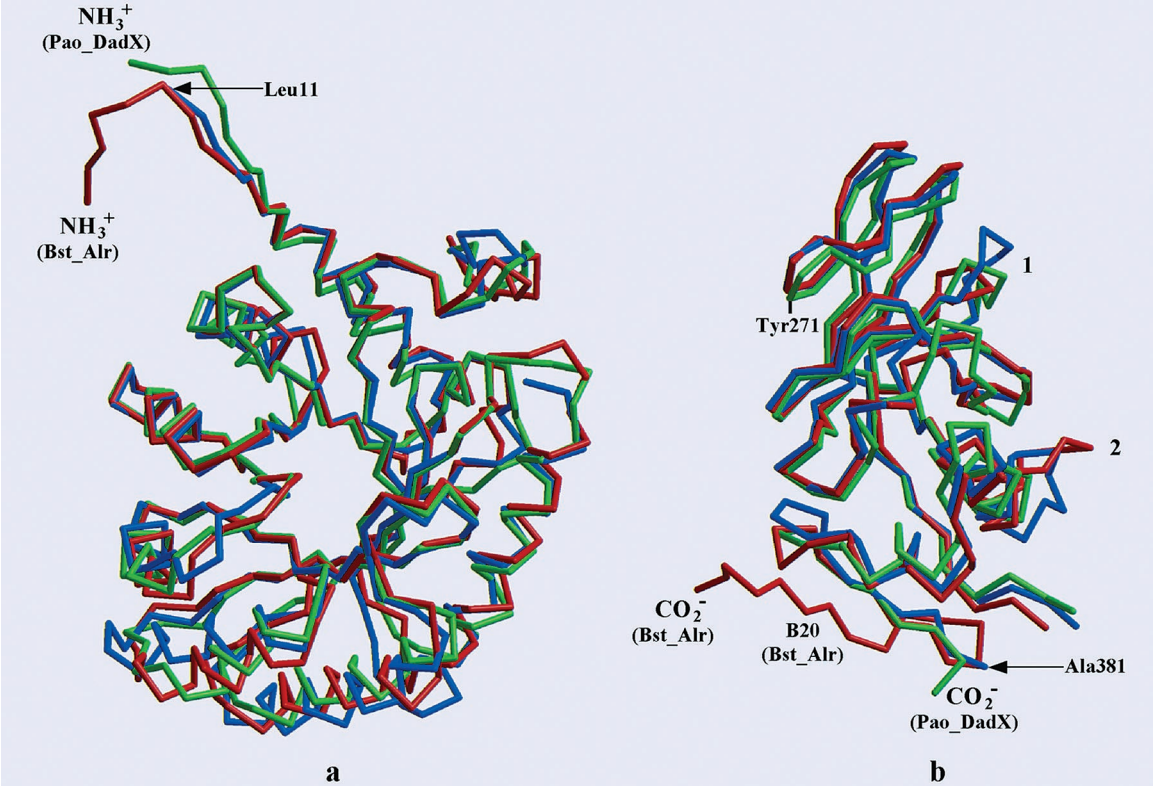

FIGURE 5: Least-squares superposition of Alr_{Mtb} (blue), $DadX_{Pao}$ (green), and Alr_{Bst} (red) obtained after a least-squares fit of the C_α atoms of (a) the N-terminal domain and (b) the C-terminal domain. Leu11 (first residue built for the N-terminal domain), Ala381 (last residue built in the C-terminal domain), and Tyr271 all are from Alr_{Mtb}. Loops labeled 1 and 2 are located in areas of large structural differences.

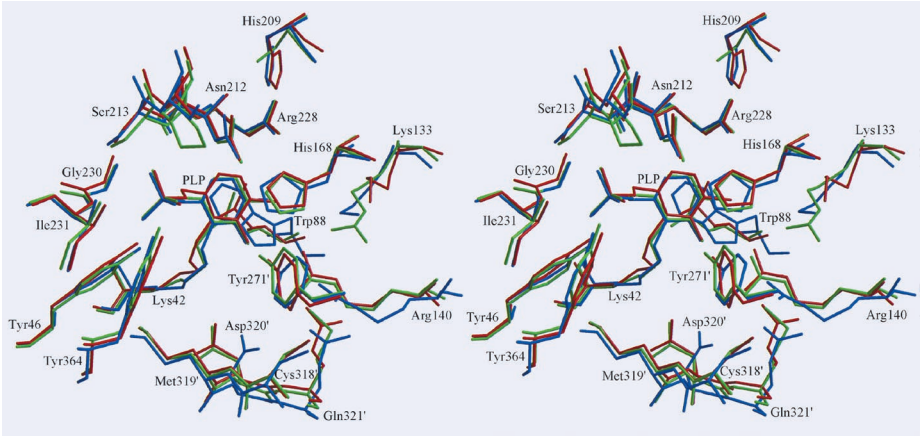

FIGURE 6: Stereoview of the superposition of the active site residues of Alr_{Mtb} (blue), $DadX_{Pao}$ (green), and Alr_{Bst} (red) obtained after a least-squares fit of the C_α atoms in the N-terminal domains. The residue numbers are those from the Alr_{Mtb} structure. Residues from the second monomer are identified with primed numbers.

(Wat203) interacts with both O3′ of PLP and NE1 of Trp88, forming a triangular hydrogen bonding network. These two waters also interact with Asp320′ and Gln321′ from the opposite monomer, as they do in the $DadX_{Pao}$ and Alr_{Bst} structures. Notably, the bulky side chain Trp88 does not alter the orientation of the strongly conserved residues found within the active site.

All bacterial alanine racemases studied to date display similar substrate specificities. This result is completely consistent with the strong structural conservation we observe within their active sites. However, it has also previously been reported by us that the V_{max} of Alr_{Mtb} is more than 100-fold lower than for either $DadX_{Pao}$ or Alr_{Bst} (*32*, *41*). Our analysis of the structure does not provide a ready explanation for this result. It is known that only the homodimeric form of alanine racemase is active (*42*). It has recently been proposed that variations in kinetic activity found for different alanine racemases may be correlated with their association constant for dimer formation (*43*). For example, in some *Shigella* species, those racemases that display tighter monomer−monomer association appeared to be more active (*43*). No data are available with regard to this hypothesis for Alr_{Mtb}.

Quality of the Electron Density throughout the Active Site. While most of the electron density is of good quality in both active sites of Alr_{Mtb}, including the PLP cofactor and the aldimine linkage (Figure 7), there is poor electron density for some residues. In active site 1 (N-terminus of monomer A and C-terminus of monomer B), six residues (174, 175,

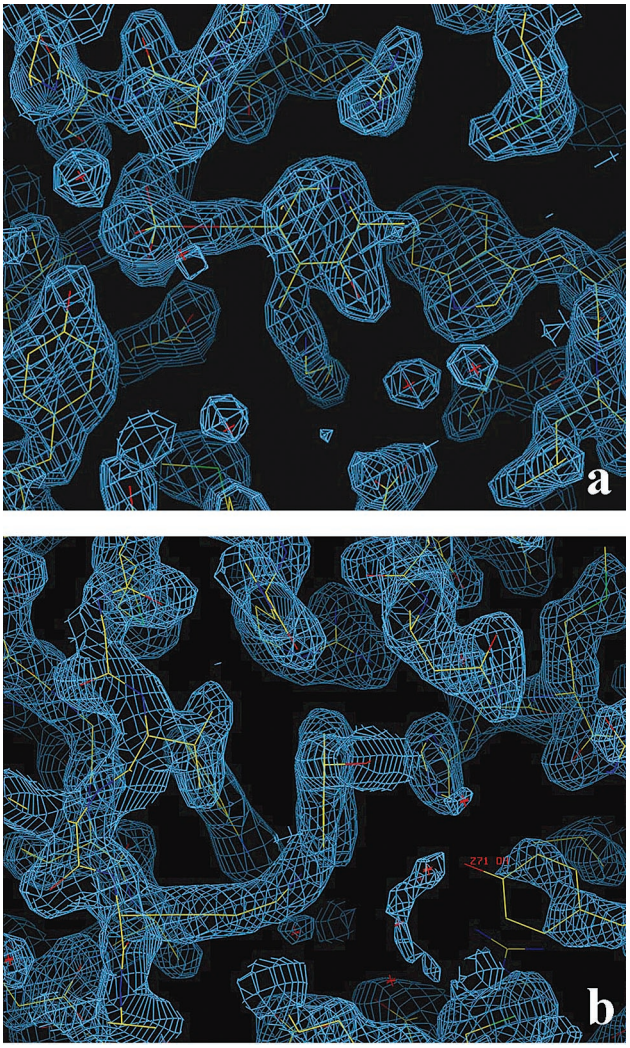

FIGURE 7: Electron density $2F_{obs} - F_{calc}$ (contoured at 2σ) maps in the active site of Alr_{Mtb} viewed when looking at the PLP cofactor (a) face view and (b) side view. Strong electron density for PLP and most surrounding residues and weaker electron density for a few other residues, such as Tyr271′ (see panel b), are apparent. The nonplanarity of the PLP−aldimine geometry is well-illustrated in panel b.

and 269′−272′) and the side chain of Arg140 are missing and residues 135−142, 172, and 173 have a high average *B* factor. In contrast, the second active site is complete, but some of the problematic residues in active site 1 also have a high *B* factor in active site 2 (N-terminus of monomer B and C-terminus of monomer A). As a result, the placement and interpretation of Tyr271′, Arg140, and Lys133 were difficult. The fact that these residues are embedded within the active site renders their disorder surprising, since the electron density for the rest of the active site is of good quality. It could suggest that the orientation and position of this three-residue system are correlated. Tyrosine 271′ is the structural equivalent of Tyr265′ in Alr_{Bst} and has been identified as one of the bases that are important in the catalytic mechanism (*23*). In Alr_{Mtb}, it could be built only in active site 2. Even then, its side chain, only roughly positioned because of poor electron density (Figure 7b), has an average *B* factor of 50.2 Å^2. Tyr271′ is actually part of a 15−20-residue region showing weak electron density in both active sites. This region comprises B13 and B14 (Figure 3) and forms a loop on the tip of which Tyr271′ is located (Figure 5b). Disorder was also observed for this tyrosine in the structures of alanine racemase complexed with acetate, propionate, and D-cycloserine (*23*, *24*), but it did not seem to affect other nearby residues. In these structures, the disorder was hypothetically related to multiple conformations for the neighboring side chain of Cys311′ (*29*).

The side chain of Arg140 was accurately located in earlier alanine racemase structures and found to be involved in strong hydrogen bonds with a nearby carbamylated lysine (*24*, *26*, *40*). Unfortunately, in Alr_{Mtb}, Arg140 is part of a region that exhibits poor electron density. Consequently, the nearby lysine in Alr_{Mtb}, Lys133, cannot be identified as a carbamylated derivative.

Orientation of PLP. The PLP cofactor and the covalently linked side chain of Lys42 have average *B* factors of 22.0 and 22.7 Å^2 in active site 1 and 22.8 and 23.8 Å^2 in active site 2, respectively. The C4′ atom of PLP, which is involved in a covalent bond with Lys42, has a somewhat higher *B* factor than the other atoms of the cofactor (28.7 Å^2 in active site 1 and 31.9 Å^2 in active site 2). The PLP is positioned such that its plane makes an angle of ∼20° with the imine bond (Figure 7b). Although the planarity between the PLP and the imine bond favors delocalization of the excess negative charge into the PLP ring upon formation of the carbanion intermediate during racemization (*44*−*46*), no such requirement is present for the internal aldimine form. In fact, this out-of-plane geometry for the imine−PLP system has been observed for the internal aldimine in several other alanine racemase structures (*23*, *24*, *26*). The lack of planarity could be an artifact due to the modest resolution of protein crystal structure determinations, but it may also suggest that small deviations from planarity in this bond system are not critical. It has been conclusively demonstrated in studies on electron delocalization in small organic compounds with extended π-systems that significant deviations from planarity are well-tolerated (*47*). Alternatively, the lack of planarity could destabilize the internal aldimine and favor the formation of the external aldimine upon encountering the substrate.

Hydrogen Bonds with PLP. Most of the hydrogen bonds with the PLP cofactor characteristic of previous alanine racemase structures are also observed in Alr_{Mtb} (Figures 8 and 9). The strong interaction between the N1 atom of PLP and a nearby arginine (Arg228) is conserved in Alr_{Mtb} at 3.0 Å. Arg228 itself is part of a four-residue hydrogen bond network comprising Tyr271′, His172, Arg228, and His209. The strong internal hydrogen bond between the imine nitrogen of Lys42 and O3′ of PLP (2.5 Å) confirms the protonated nature of the Schiff base. The phosphate tail of PLP is held in place by a total of six hydrogen bonds, identical to those observed in previously determined structures. However, as described above, poor electron density for some residues interferes with a complete analysis of the hydrogen bond network.

One new hydrogen bond noted in this structure involves the O3′ atom of PLP with the NE1 atom of Trp88. This 3.3 Å interaction is not observed in the $DadX_{Pao}$ and Alr_{Bst} structures where Trp88 is replaced with Leu85 and Leu78, respectively. Note that among the residues involved in hydrogen bonding with and around PLP in all three alanine racemases, only a few are not fully conserved. For Alr_{Mtb}, they are Trp88, Leu89, and Asn141 as shown below. These

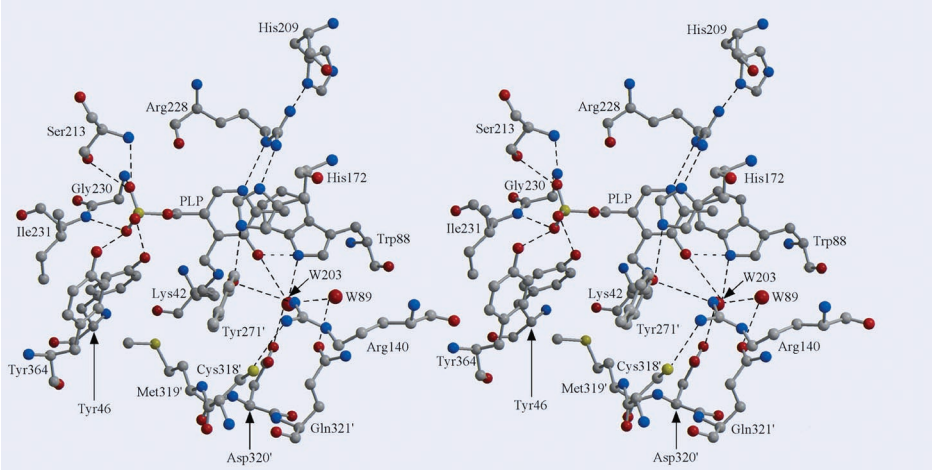

FIGURE 8: Stereoview of the hydrogen bond network in the active site of Alr_{Mtb}.

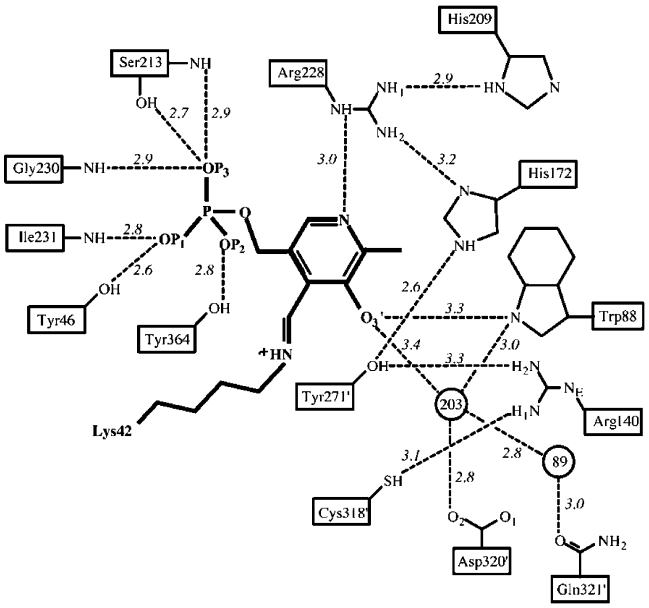

FIGURE 9: Schematic diagram of the hydrogen bond network in the active site of Alr_{Mtb}.

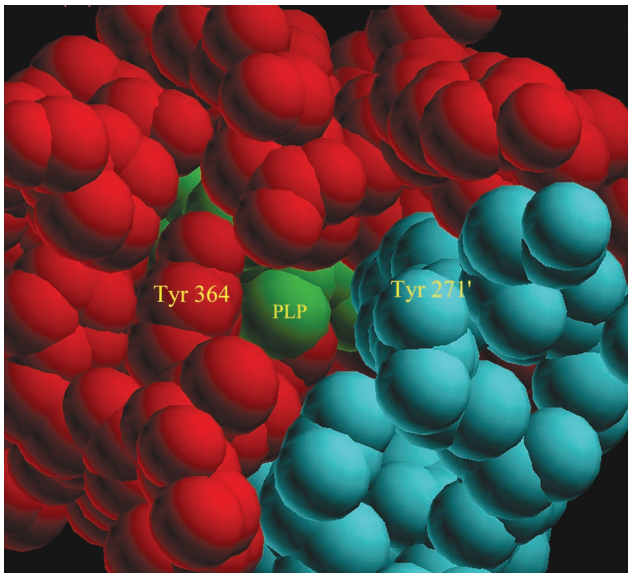

FIGURE 10: Space-filling representation of the constricted entryway to the binding pocket of Alr_{Mtb}. The tyrosines labeled Tyr364 and Tyr271′ must be traversed in route to the active site PLP.

three residues are all part of the second cavity described above.

Conserved Entryway into the Active Site. The substrate binding site itself is compact (5.5 Å × 5.0 Å × 2.5 Å) and located near the PLP molecule. Although it is large enough to allow successful docking of molecules in the molecular weight range of 300, it is difficult for these molecules to reach the compact active site because of a constriction in the entryway corridor formed near the PLP by two residues, Tyr271′ and Tyr364 (Figure 10). The entryway corridor is roughly conical with its base oriented toward the outside of the enzyme. This entryway narrows as the PLP is approached.

The corridor to the active site in alanine racemase can be thought of as three layers, outer, middle, and inner, with the inner layer terminating at the PLP. The construction of these layers is shown schematically in Table 4. The outer layer in AlrMtb contains three residues, Asp357, Lys178, and Ala241. The middle layer contains Arg316′, Ile362, Arg296′, and Asp177, while the inner layer contains Tyr271′, Tyr364, Tyr290′, and Ala176. This inner layer contains the two tyrosines, Tyr271′ and Tyr364, that gate the entrance of D-Ala and inhibitors to the PLP binding cavity. These two residues define an opening of ~2.7 Å in the crystal structure and most certainly must move apart to permit small substances to enter and leave the active site (Figure 10). The residues

Table 4: Residues Lining the Entrance Corridor in Alr_{Mtb}, $DadX_{Pao}$, and Alr_{Bst}[a]

outer mid inner PLP

position	Alr_{Mtb}	$DadX_{Pao}$	Alr_{Bst}
	Inner Layer		
1	Tyr271′	Tyr253′	Tyr265′
2	Tyr364	Tyr341	Tyr354
3	Tyr290′	Tyr272′	Tyr284′
4	Ala176	Ala162	Ala170
	Middle Layer		
1	Arg316′	Arg298′	Arg309′
2	Ile362	Ile339	Ile352
3	Arg296′	Arg278′	Arg290′
4	Asp177	Asp163	Asp171

[a] Primed numbers are residues contributed by the opposite monomer.

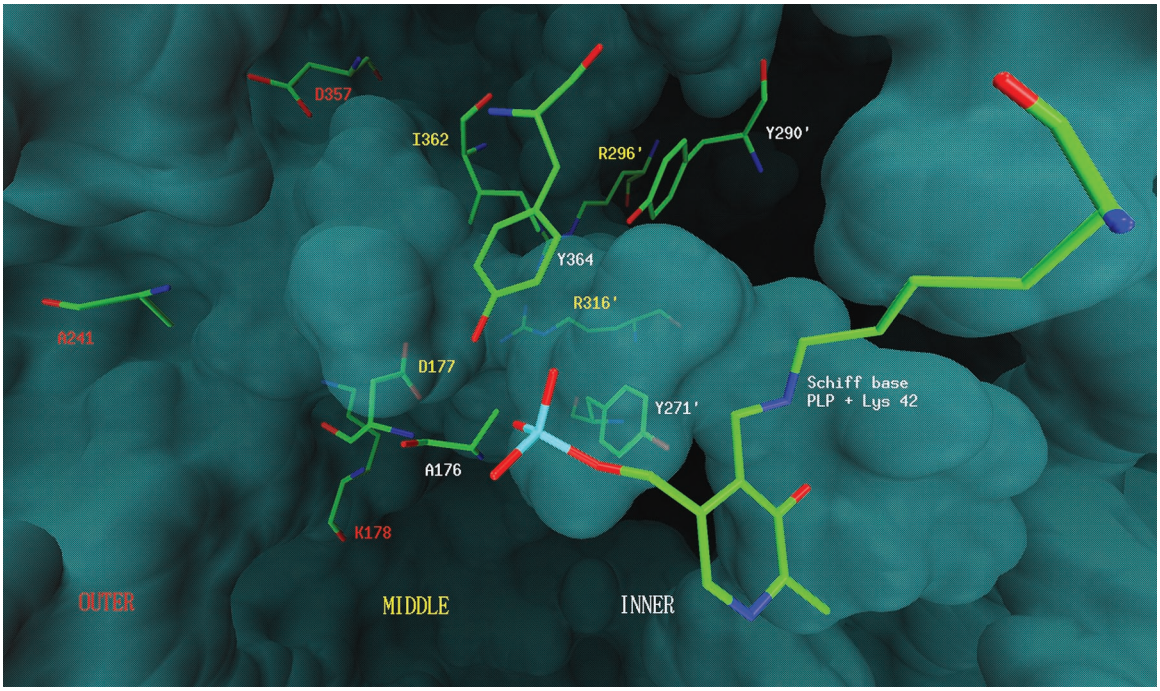

FIGURE 11: Depiction of the binding cavity for Alr_{Mtb} viewed from within the enzyme with obstructing residues removed. This cavity begins at the surface of the enzyme and progresses from left to right, traversing the outer, middle, and inner layers of residues until reaching the PLP. Residues from the outer layer are labeled with red text, those from the middle layer with yellow, and those from the inner layer with white. Residues in the middle and inner layers are strongly conserved. To the right of the PLP cofactor, the secondary pocket can also be seen (see the text).

located in each layer of the corridor are shown in Figure 11.

To date, most known inhibitors of alanine racemase bind solely to the substrate binding region proximal to the PLP. Another way to approach the problem of drug design for inhibiting alanine racemase would be to include residues from this corridor in an extended pharmacophore model. Now that several structures of alanine racemase are available for comparison, we have discovered that the inner and middle layers of this corridor are strongly conserved across species. This conservation supports the inclusion of these residues in the drug design process. A comparison of this corridor region, sorted by layer, in the structures of alanine racemase in *M. tuberculosis*, *G. stearothermophilus*, and *P. aeruginosa* is shown in Table 4. In the inner and middle layers, all four residues are identical and they are located similarly around the corridor. Residues in the outer layer near the surface of the enzyme are not conserved. Having noticed this strongly conserved structural motif, we proceeded to create ClustalW alignments to screen all the alanine racemase sequences deposited in GenBank for correlation with our model. With very few exceptions (data not shown), all sequences examined, from both Gram-negative and Gram-positive bacteria, contain identical residues at the positions in question. Also, the presence of these residues in individual alanine racemases is independent of their overall relatedness. For instance, the 69% overall identical *Mycobacterium smegmatis* sequence shares the identical inner and middle layer residues with the *M. tuberculosis* sequence, as does the *Bordetella pertussis* alanine racemase, which is overall only 31% identical to Alr_{Mtb}. This result further emphasizes the importance of including the corridor region in the drug design process, thus, resulting in greater flexibility in inhibitor design. A sample docking of a small molecule inhibitor candidate within the alanine racemase corridor is shown in Figure 12 and illustrates that inhibitor molecules larger than alanine are easily accommodated within this framework.

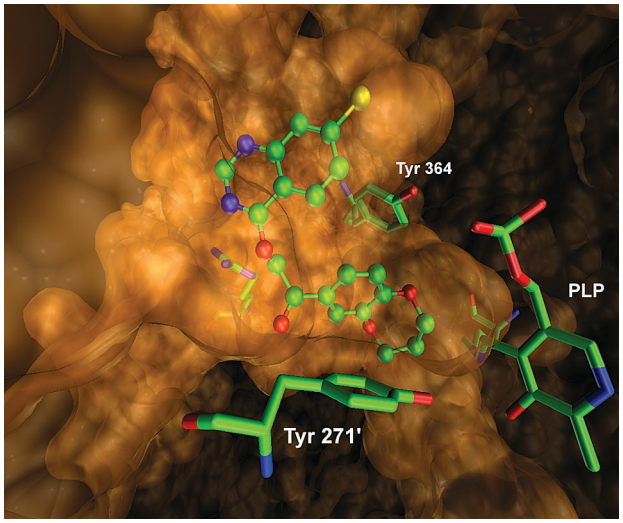

FIGURE 12: Depiction of an inhibitor candidate, 2-[(7-chloro-4-quinazolinyl)oxy]-1-(3,4-dihydro-2*H*-1,5-benzodioxepin-7-yl)-1-ethanone, chosen to utilize the entrance as well as the active site of the enzyme. In principle, this approach will allow for larger and more specific inhibitors of alanine racemase to be identified. The compound was docked using AutoDock (*49*). The docking procedure involved using the Lamarckian genetic search algorithm using a population size of 50 with a total of 100 separate docking runs. The docking orientation for the ligand−macromolecule complex presented here was one from the most populated cluster containing 35 members (using a root-mean-square tolerance of 1.5 Å for clustering the docked ligand poses) with a docking energy of −11.01 kcal/mol.

Other groups have proposed similar strategies for developing inhibitors for enzymes with long entryways into their active sites (*48*). For example, a histone deacetylase-like

protein has been the target of structure-aided drug design efforts because of its role in the transcriptional process. It is unrelated to alanine racemase except that it also contains a long passageway from the exterior of the enzyme into the active site. Recently, the development of inhibitors that target multiple sites within this enzyme, including the outer pocket, inner corridor, and internal active site, has been proposed (*48*). It is felt that these inhibitors may have significant advantages over those that target only a single site within the enzyme.

CONCLUSION

Analysis of the Alr_{Mtb} structure confirms once more that this enzyme remains a challenging but important target for drug design against tuberculosis. We now have a structure of the actual macromolecule that is the clinical target of D-cycloserine, an important antibiotic for use against drug resistant TB. The structure is very similar to the alanine racemase structures known from *Geobacillus* and *Pseudomonas*. The hinge angles between the monomer domains of all three structures are unique, but key active site residues superimpose well. The most significant result to come from this structural report involves the entryway that leads to the active site. Our analysis reveals that the inner and middle regions of this corridor are strongly conserved across species, while regions near the enzyme surface are more variable. Drug design trials that target features within the entryway as well as the active site pocket are now underway in our laboratories.

ACKNOWLEDGMENT

Use of the Advanced Photon Source was supported by the U.S. Department of Energy, Basic Energy Sciences, Office of Science, under Contract W-31-109-Eng-38. Use of the BioCARS Sector 14 was supported by the National Institutes of Health, National Center for Research Resources, under Grant RR07707. In addition, some of this work is based upon research conducted at the Cornell High Energy Synchrotron Source (CHESS), which is supported by the National Science Foundation under Grant DMR 97-13424, using the Macromolecular Diffraction at CHESS (MacCHESS) facility, which is supported by Grant RR-01646 from the National Institutes of Health, through its National Center for Research Resources. We also thank the Institute of Molecular Design and Accelrys, Inc., for the use of computational resources. We acknowledge Kevin McGrory and Hung-Chung Huang for their technical assistance and expertise.

REFERENCES

1. Dye, C., Garnett, G. P., Sleeman, K., and Williams, B. G. (1998) Prospects for worldwide tuberculosis control under the WHO DOTS strategy. Directly observed short-course therapy, *Lancet 352*, 1886−1891.
2. World Health Organization (2002) Fact Sheet No 104: Tuberculosis, *WHO Fact Sheets*, World Health Organization, Geneva.
3. Bloom, B. R. (1994) *Tuberculosis: Pathogenesis, Protection, and Control*, American Society for Microbiology Press, Washington, DC.
4. Musser, J. M. (1995) Antimicrobial agent resistance in mycobacteria: Molecular genetic insights, *Clin. Microb. Rev. 8*, 496−514.
5. Mahmoudi, A., and Iseman, M. D. (1993) Pitfalls in the care of patients with tuberculosis. Common errors and the association with the acquisition of drug resistance, *J. Am. Med. Assoc. 270*, 65−68.
6. Pablos-Mendez, A. R. M., Laszlo, A., Binkin, N., Rieder, H. L., Bustreo, F., Cohn, D. L., Lambregts-van Weezenbeek, C. S., Kim, S. J., Chaulet, P., and Nunn, P. (1998) Global surveillance for antituberculosis-drug resistance, 1994−1997. World Health Organization-International Union against Tuberculosis and Lung Disease Working Group on Anti-Tuberculosis Drug Resistance Surveillance, *N. Engl. J. Med. 338*, 1641−1649.
7. Salomon, N., Perlman, D. C., Friedmann, P., Buchstein, S., Kreiswirth, B. N., and Mildvan, D. (1995) Predictors and outcome of multidrug-resistant tuberculosis, *Clin. Infect. Dis. 21*, 1245−1252.
8. Portaels, F. R. L., and Bastian, I. (1999) Addressing multidrug-resistant tuberculosis in penitentiary hospitals and in the general population of the former Soviet Union, *Int. J. Tuberc. Lung Dis. 3*, 582−588.
9. Goble, M., Iseman, M. D., and Madsen, L. A. (1993) Treatment of 171 patients with pulmonary tuberculosis resistant to isoniazid and rifampin, *N. Engl. J. Med. 328*, 527−532.
10. Iseman, M. D. (1993) Treatment of multi-drug resistant tuberculosis, *N. Engl. J. Med. 329*, 784−791.
11. National Institutes of Health (2003) Biodefense Research Agenda for Category B and C Priority Pathogens, NIH Publication 03-5315, National Institutes of Health, Bethesda, MD.
12. Cole, S. T., Brosch, R., Parkhill, J., Garnier, T., Churcher, C., Harris, D., Gordon, S. V., Eiglmeier, K., Gas, S., Barry, C. E., III, Tekaia, F., Badcock, K., Basham, D., Brown, D., Chillingworth, T., Connor, R., Davies, R., Devlin, K., Feltwell, T., Gentles, S., Hamlin, N., Holroyd, S., Hornsby, T., Jagels, K., Barrell, B. G., et al. (1998) Deciphering the biology of *Mycobacterium tuberculosis* from the complete genome sequence, *Nature 393*, 537−544.
13. UCLA-DOE Institute for Genomics and Proteomics (2003) The Mycobacterium Tuberculosis Structural Genomics Consortium (http://www.doe-mbi.ucla.edu/TB/index.php).
14. National Institutes of Health (2004) Protein Structure Initiative (http://www.nigms.nih.gov/psi/centers.html#tb).
15. Lambert, M. P., and Neuhaus, M. P. (1972) Mechanism of D-Cycloserine Action: Alanine Racemase from *Escherichia coli*, *J. Bacteriol. 110*, 978−987.
16. Silverman, R. B. (1988) The Potential use of Mechanism-Based Enzyme Inactivators in Medicine, *J. Enzyme Inhib.*, 73−90.
17. Copie, V., Faraci, W. S., Walsh, C. T., and Griffin, R. G. (1988) Inhibition of Alanine Racemase by Alanine Phosphonate: Detection of an Imine Linkage to Pyridoxal 5′-Phosphate in the Enzyme Inhibitor Complex by Solid-State ^{15}N Nuclear Magnetic Resonance, *Biochemistry 27*, 4966−4970.
18. Walsh, C. (2003) in *Antibiotics: Actions, origins, resistance*, pp 23−49, American Society for Microbiology Press, Washington, DC.
19. Weinstein, L. (1975) in *The Pharmacological Basis of Therapeutics* (Goodman, L. S., and Gilman, A., Eds.) 5th ed., pp 1202−1223, Macmillan Publishing, New York.
20. Newton, R. W. (1975) Side Effects of Drugs Used to Treat Tuberculosis, *Scott. Med. J. 20*, 47−49.
21. Yew, W. W., Wong, C. F., Wong, P. C., Lee, J., and Chau, C. H. (1993) Adverse Neurological Reactions in Patients with Multidrug-Resistant Pulmonary Tuberculosis after Coadministration of Cycloserine and Ofloxacin, *Clin. Infect. Dis. 42*, 14752−14761.
22. Katz, M. H. (1994) Effect of HIV Treatment on Cognition, Behavior, and Emotion, *Psychiatry Clin. North Am. 17*, 227−230.
23. Shaw, J. P., Petsko, G. A., and Ringe, D. (1997) Determination of the Structure of Alanine Racemase from *Bacillus stearothermophilus* at 1.9 Å Resolution, *Biochemistry 36*, 1329−1342.
24. Morollo, A. A., Petsko, G. A., and Ringe, D. (1999) Structure of a Michaelis Complex Analogue: Propionate Binds in the Substrate Carboxylate Site of Alanine Racemase, *Biochemistry 38*, 3293−3301.
25. Ondrechen, M. J., Briggs, J. M., and McCammon, J. A. (2001) A Model for Enzyme-Substrate Interaction in Alanine Racemase, *J. Am. Chem. Soc. 123*, 2830−2834.
26. Le Magueres, P., Im, H., Dvorak, A., Strych, U., Benedik, M., and Krause, K. L. (2003) Crystal Structure at 1.45 Å of Alanine Racemase from a Pathogenic Bacterium, *Pseudomonas aerugi-*

nosa, Contains Both Internal and External Aldimine Forms, *Biochemistry 42*, 14752−14761.
27. Watanabe, A., Yoshimura, T., Mikami, B., and Esaki, N. (1999) Tyrosine 265 of Alanine Racemase Serves as a Base Abstracting a Hydrogen from L-Alanine: The Counterpart Residue to Lys39 Specific to D-Alanine, *J. Biochem. 126*, 781−786.
28. Stamper, C. G. F., Morollo, A. A., and Ringe, D. (1998) Reaction of Alanine Racemase with 1-Aminoethylphophonic Acid Forms a Stable External Aldimine, *Biochemistry 37*, 10438−10445.
29. Fenn, T. D., Stamper, G. F., Morollo, A. A., and Ringe, D. (2003) A side Reaction of Alanine Racemase: Transamination of Cycloserine, *Biochemistry 42*, 5775−5783.
30. Olson, G. T., Mengmeng, F., Lau, S., Rinehart, K. L., and Silverman, R. B. (1998) An Aromatization Mechanism of Inactivation of γ-Aminobutyric Acid Aminotransferase for the Antibiotic L-Cycloserine, *J. Am. Chem. Soc. 120*, 2256−2267.
31. Peisach, D., Chipman, D. M., Van Ophem, P. W., Manning, J. M., and Ringe, D. (1998) D-Cycloserine Inactivation of D-Amino Acid Aminotransferase Leads to a Stable Noncovalent Protein Complex with an Aromatic Cycloserine-PLP Derivative, *J. Am. Chem. Soc. 120*, 2268−2274.
32. Strych, U., Penland, R. L., Jimenez, M., Krause, K. L., and Benedik, M. J. (2001) Characterization of the Alanine Racemase from Two Mycobacteria, *FEMS Microbiol. Lett. 196*, 93−98.
33. Otwinowski, Z., and Minor, W. (1997) in *Methods in Enzymology* (Carter, C. W., Jr., and Sweet, R. M., Eds.) pp 307−326, Academic Press, New York.
34. Terwilliger, T. C., and Berendzen, J. (1999) Automated Structure Solution for MIR and MAD, *Acta Crystallogr. D55*, 849−861.
35. Perrakis, A., Sixma, T. K., Wilson, K. S., and Lamzin, V. S. (1997) wARP: Improvement and Extension of Crystallographic Phases by Weighted Averaging of Multiple Refined Dummy Atomic Models, *Acta Crystallogr. D53*, 448−455.
36. Perrakis, A., Morris, R. J., and Lamzin, V. S. (1999) Automated Protein Model Building Combined with Iterative Structure Refinement, *Nat. Struct. Biol. 6*, 458−463.
37. Lamzin, V. S., and Wilson, K. S. (1997) Automated Refinement for Protein Crystallography, *Methods Enzymol. 277*, 269−305.
38. Sheldrick, G. M., and Schneider, T. R. (1997) Shelxl: High-Resolution Refinement, *Methods Enzymol. 277*, 319−343.
39. Jones, T. A., Zou, J. Y., Cowan, S. W., and Kjeldgaard, M. (1991) Improved Methods for Building Protein Models in Electron Density Maps and the Location of Errors in these Models, *Acta Crystallogr. A47*, 110−119.
40. Watanabe, A., Yoshimura, T., Mikami, B., Hayashi, H., Kagamiyama, H., and Esaki, N. (2002) Reaction mechanism of alanine racemase from *Bacillus stearothermophilus*: X-ray crystallographic studies of the enzyme bound with *N*-(5′-phosphopyridoxyl)alanine, *J. Biol. Chem. 277*, 19166−19172.
41. Strych, U., Huang, H. C., Krause, K. L., and Benedik, M. J. (2000) Characterization of the alanine racemases from *Pseudomonas aeruginosa* PAO1, *Curr. Microbiol. 41*, 290−294.
42. Strych, U., and Benedik, M. J. (2002) Mutant analysis shows that alanine racemases from *Pseudomonas aeruginosa* and *Escherichia coli* are dimeric, *J. Bacteriol. 184*, 4321−4325.
43. Yokoigawa, K., Okubo, Y., and Soda, K. (2003) Subunit interaction of monomeric alanine racemase from four Shigella species in catalytic reaction, *FEMS Microbiol. Lett. 221*, 263−267.
44. Yano, T., Kuramiysu, S, Tanase, S., Morino, Y., and Kagamiyama, H. (1992) Role of Asp222 in the Catalytic Mechanism of *Escherichia coli* Aspartate Aminotransferase: The Amino Acid Residue Which Enhances the Function of the Enzyme-bound Coenzyme Pyridoxal 5′-Phosphate, *Biochemistry 31*, 5878−5887.
45. Arnone, A., Christen, P., Jansonius, J. N., and Metzler, D. E. (1985) in *Transaminases* (Christen, P., and Metzler, D. E., Ed.) pp 326−357, John Wiley & Sons, New York.
46. McPhalen, C. A., Vincent, M. G., and Jansonius, J. N. (1992) X-ray Structure Refinement and Comparison of Three Forms of Mitochondrial Aspartate Aminotransferase, *J. Mol. Biol. 225*, 495−517.
47. Lindeman, S. V., Rosokha, S. V., Sun, D. L., and Kochi, J. K. (2002) X-ray structure analysis and the intervalent electron transfer in organic mixed-valence crystals with bridged aromatic cation radicals, *J. Am. Chem. Soc. 124*, 843−855.
48. Wang, D.-F., Wiest, O., Helquist, P., Lan-Hargest, H.-Y., and Wiech, N. L. (2004) On the Function of the 14 Å Long Internal Cavity of Histone Deacetylase-Like Protein: Implications for the Design of Histone Deacetylase Inhibitors, *J. Med. Chem. 47*, 3409−3417.
49. Goodsell, D. S., Morris, G. M., and Olson, A. J. (1996) Automated docking of flexible ligands: Applications of AutoDock, *J. Mol. Recognit. 9*, 1−5.

BI0486583